Magnetic anisotropy of embedded Co nanoparticles: Influence of the surrounding matrix

Alexandre Tamion,[1] Cécile Raufast,[1] Matthias Hillenkamp,[1,2,*] Edgar Bonet,[3] J. Jouanguy,[4] Bruno Canut,[5] Estella Bernstein,[1] Olivier Boisron,[1] Wolfgang Wernsdorfer,[3] and Véronique Dupuis[1]

[1]*University Lyon 1, Laboratoire de Physique de la Matière Condensée et Nanostructures, CNRS–University of Lyon, UMR 5586, 69622 Villeurbanne, France*

[2]*University Lyon 1, Laboratoire de Spectrométrie Ionique et Moléculaire, CNRS–University of Lyon, UMR 5579, 69622 Villeurbanne, France*

[3]*Institut Néel, CNRS and University Joseph Fourier, BP 166, 25 Avenue des Martyrs, 38042 Grenoble Cedex 9, France*

[4]*Unite EPHYSE, INRA, 71, Avenue Edouard Bourlaux, 33140 Villenave d'Ornon, France*

[5]*University Lyon 1, Lyon Institute of Nanotechnology, CNRS UMR 5270, University of Lyon, F-69622 Villeurbanne Cedex, France*

(Received 4 December 2009; revised manuscript received 12 February 2010; published 5 April 2010)

We report on the magnetic properties of Co clusters embedded in four different matrices (Ag, Au, Si, and amorphous carbon). The recently developed "triple fit" method for treating conventional magnetometry data allows, together with micro-superconducting quantum interference device (μ-SQUID) investigations, the detailed study of the influence of the surrounding matrix on the magnetic volume and the magnetic anisotropy of Co nanoparticles. While interdiffusion between matrix and Co atoms cannot be excluded in Si and amorphous C matrices, the structure of clusters embedded in the metallic matrices remains intact. Ag and Au matrices increase significantly the magnetic anisotropy energy of the Co clusters. μ-SQUID experiments indicate that the magnetic anisotropy of embedded clusters is not affected by a magnetically dead layer and that an anisotropy dispersion must be taken into account for size-selected nanoparticles.

DOI: 10.1103/PhysRevB.81.144403 PACS number(s): 36.40.Cg, 75.50.Tt, 81.07.−b

I. INTRODUCTION

Magnetic nanoparticles have attracted a lot of attention both for their fundamental interest as well as for their potential applications. In particular, these nanoparticles might be used in future high-density magnetic storage media.[1] However, on the nanometer scale, the magnetization direction of a particle below a certain size fluctuates at ambient temperature, the particle is superparamagnetic. One of the main challenges in this field of research is the attempt to push the limit of superparamagnetism[2] toward as small as possible particles by increasing the nanoparticle's magnetic anisotropy energy (MAE).[3]

This MAE has two principal contributions. On the one hand, the volume anisotropy is mainly determined by the particle's crystallographic structure via the magnetocrystalline anisotropy. But high-symmetry structures such as fcc do not favor a high magnetocrystalline anisotropy in Co nanoparticles.[4] On the other hand, the surface anisotropy has two origins. First, as the lower coordinated atoms at the surface are in a less symmetric environment, they enhance the MAE as compared to the bulk.[4,5] Second, the contact with a nonferromagnetic matrix can induce an interfacial anisotropy, whose origin depends on the detailed electronic structure of the nanoparticle and the matrix. For example, in the case of metallic matrices, the interfacial anisotropy is due to the spin-orbit coupling and hybridization between cluster and matrix orbitals, as already shown in Co/Pt multilayers[6] or Co clusters embedded in Pt matrices.[7]

In this study, we present magnetic measurements of noninteracting Co clusters embedded in four different matrices: amorphous carbon (a-C), semiconducting silicon, and two noble-metal matrices (Ag and Au). Using the "triple fit" method,[8] we show that both the MAE and the median magnetic diameter of well-characterized clusters assemblies change drastically depending on the matrix nature. In order to try to determine the intrinsic MAE distribution, we compare these data to low-temperature micro-superconducting quantum interference device (μ-SQUID) measurement on individual Co clusters in an a-C matrix.

II. SAMPLE PREPARATION AND CHARACTERIZATION

Samples are prepared from preformed gas-phase clusters following the low-energy cluster beam deposition technique.[9] Briefly, metal clusters are produced in a laser vaporization-gas condensation source. The plasma is created by the impact of a Nd:YAG (yttrium aluminum garnet) laser beam focused on a Co rod, and thermalized by injection of a continuous flow of helium at low pressure inducing the cluster growth. Next, the clusters are cooled down in a supersonic expansion at the exit nozzle of the source. The obtained low-energy cluster beam is then codeposited together with the atomic beam for the matrix under ultrahigh-vacuum conditions (10^{-10} mbar static pressure, 10^{-8} mbar He during deposition). This codeposition technique protects metal clusters from oxidation and allows us to independently adjust the cluster size and concentration.

As shown in Fig. 1, the diameter *probability density function* (PDF) of the deposited clusters, as deduced from transmission electron microscopy (TEM) observations, closely follows a lognormal curve with a relative sharp dispersion,

$$\mathrm{PDF}(D) = \frac{1}{w\sqrt{2\pi}}\frac{1}{D}\exp\left[-\frac{1}{2}\left(\frac{\log(D/D^m)}{w}\right)^2\right].$$

The derived median diameter is $D^m = (3.2 \pm 0.1)$ nm and the dispersion is $w = 0.3 \pm 0.05$.

Further sample characterization was obtained by Rutherford backscattering spectrometry (RBS) in order to quantita-

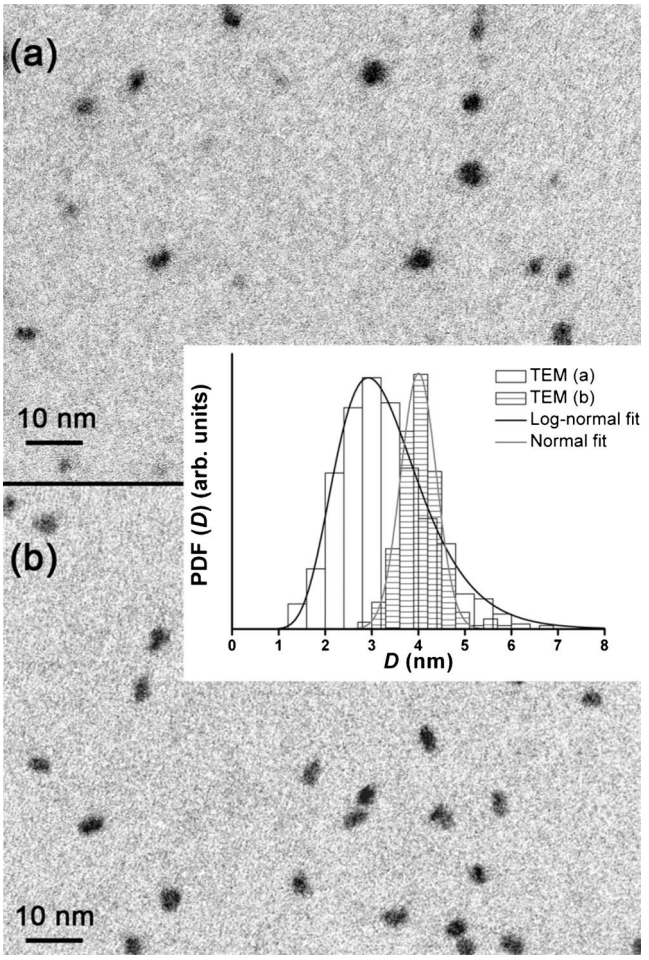

FIG. 1. TEM images of (a) nonsize-selected and (b) size-selected Co clusters embedded in amorphous carbon. The inset displays the deduced size histograms, together with the best fits corresponding to a lognormal and Gaussian size distribution. The fit parameters are $D^m=(3.2\pm0.1)$ nm and $w=0.3\pm0.05$ for (a) and $D^m=(4.0\pm0.1)$ nm and $w=0.09\pm0.01$ for (b).

tively check the atomic composition [Co]/[C]. The analysis was performed with $^4He^+$ ions of 2 MeV energy delivered by the 4 MV Van de Graaff accelerator of the Nuclear Physics Institute of Lyon (IPNL). The backscattered particles were detected with a 13 keV resolution implanted junction set at an angle of 172° with respect to the beam axis.

Figure 2 shows the RBS spectrum recorded on a Co:a-C sample. The signals related to carbon and cobalt species are clearly visible. The presence of sharp steps, with uniformly varying plateaux, indicates a low surface roughness and a good homogeneity in depth. Within the analysis accuracy, no significant contamination with oxygen can be depicted in the film. With the help of the SIMNRA simulation code,[10] we extracted from the experimental data the average stoichiometry $Co_{0.01}C_{0.99}$, in good agreement with the expected volumic composition of the sample.

Great care has been taken to minimize direct and indirect interactions between nanoparticles that prevent unambiguous interpretation of magnetization data.[8,11] It has been found crucial to truly codeposit clusters and matrix atoms in a random three-dimensional film since samples prepared by alternating cluster and matrix layers often display significant deviations from superparamagnetic behavior due to magnetic interparticle interactions. The results shown here were obtained for samples with 1 vol % Co, a dilution that did not display any signs of interaction for nanoparticles of the size used here (around 3 nm) even in the most sensitive triple fit treatment, as detailed below.

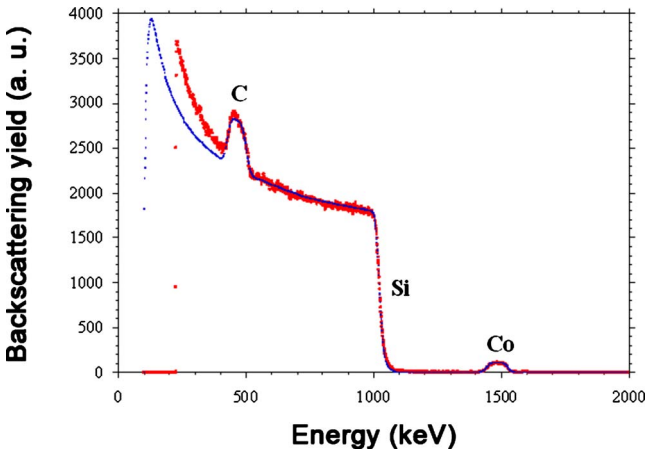

FIG. 2. (Color online) RBS spectrum (red points) and corresponding SIMNRA simulation (blue points) of the Co:a-C sample on a Si substrate.

Based on the nanoparticle diameter PDF and the concentration, we simulated the random composition of our samples in order to quantify the mean interparticle distances, crucial for an estimation of interactions.

This simulation presented in Fig. 3 shows that the clusters are well separated and yields a mean distance between nearest neighbors of 7.9 nm center to center and 4.5 nm surface to surface. The ratio of clusters in direct contact (distance lower than 0.14 nm) is close to 0.35%. We consequently

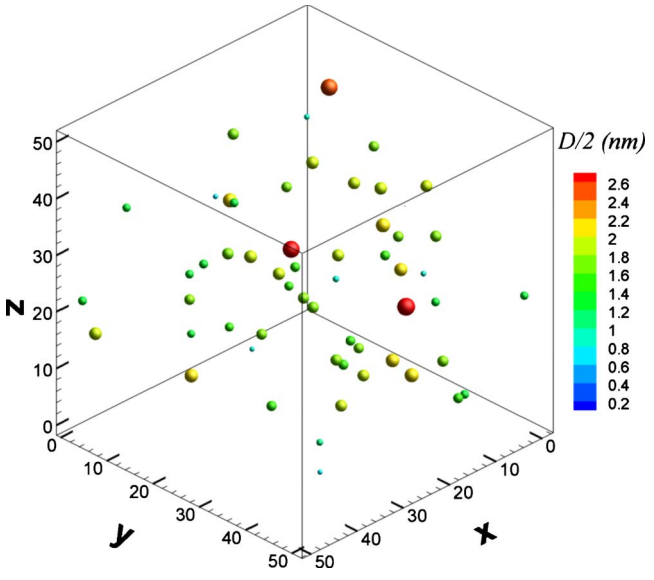

FIG. 3. (Color online) Simulation of our samples: 1% Co according to the cluster diameter PDF as derived from TEM, randomly arranged in a box with 50 nm edges. The colors illustrate the particle size.

neglect interparticle interactions, which is also confirmed by the magnetic measurements described below.

III. RESULTS

A. Magnetometry

All the magnetic measurements have been performed using a superconducting quantum interference device (SQUID) magnetometer (Quantum Design MPMS 5 XL) at various temperatures. The diamagnetic response of the silicon substrate has been thoroughly characterized and all curves are corrected for this contribution. Note that the particle ensembles studied here are not necessarily fully saturated at 300 K and 5 T.

The high-temperature (300 K) hysteresis loops (see Fig. 4) do not show any coercivity, which is typical of an assembly of superparamagnetic particles. On the other hand, magnetization loops at low temperature (2 K, not shown) exhibit coercivity and a remanent magnetic moment. In accordance with the Stoner-Wohlfarth model for an assembly of randomly oriented macrospins without interactions, the ratio between remanent and saturated magnetization is lower than 0.5 (Ref. 12) for parallel and perpendicular orientation of the applied magnetic field with respect to the sample plane. A further corroboration for independent superparamagnetic macrospins is the fact that the magnetization curves at $T \geq 200$ K overlap when plotted as a function of H/T. We would like, however, to stress the fact that these simple checks, while necessary, are not sufficient to exclude interactions. We have found our triple fit method (see below) to be much more sensitive to deviations from pure superparamagnetic behavior.

We have also performed magnetic-susceptibility measurements following the zero-field-cooled/field-cooled (ZFC/FC) procedure in order to quantitatively determine the anisotropy constant for Co nanoparticles embedded in different matrices. As can be seen in Fig. 4, the ZFC curves show the transition from the ferromagnetic to the superparamagnetic regime, as evidenced by a susceptibility peak around a given temperature T_{max}.

B. Micromagnetometry

In order to further narrow down the different possible influences of the surrounding matrix on the magnetic anisotropy of embedded clusters, we have also performed measurements of individual particles using the micro-SQUID technique.[5] Here mass-selected Co clusters[13,14] were deposited at very low density (<1 at. %) in a carbon matrix on top of a superconducting Nb film. These samples were subsequently patterned into μ-SQUIDs. The magnetic flux coupling of clusters located directly above the Josephson junctions is strong enough to detect the individual magnetization reversals induced by an applied magnetic field, using the micro-SQUID as a sensor. The angular dependence of the static switching field at low temperature ($T=35$ mK) closely follows the predicted Stoner-Wohlfarth astroid (see Fig. 5), in good agreement with a uniform rotation of the cluster magnetization.[15] Astroids of four different nanoparticles can be discerned, all of them with their easy axes in or close to the sample plane.

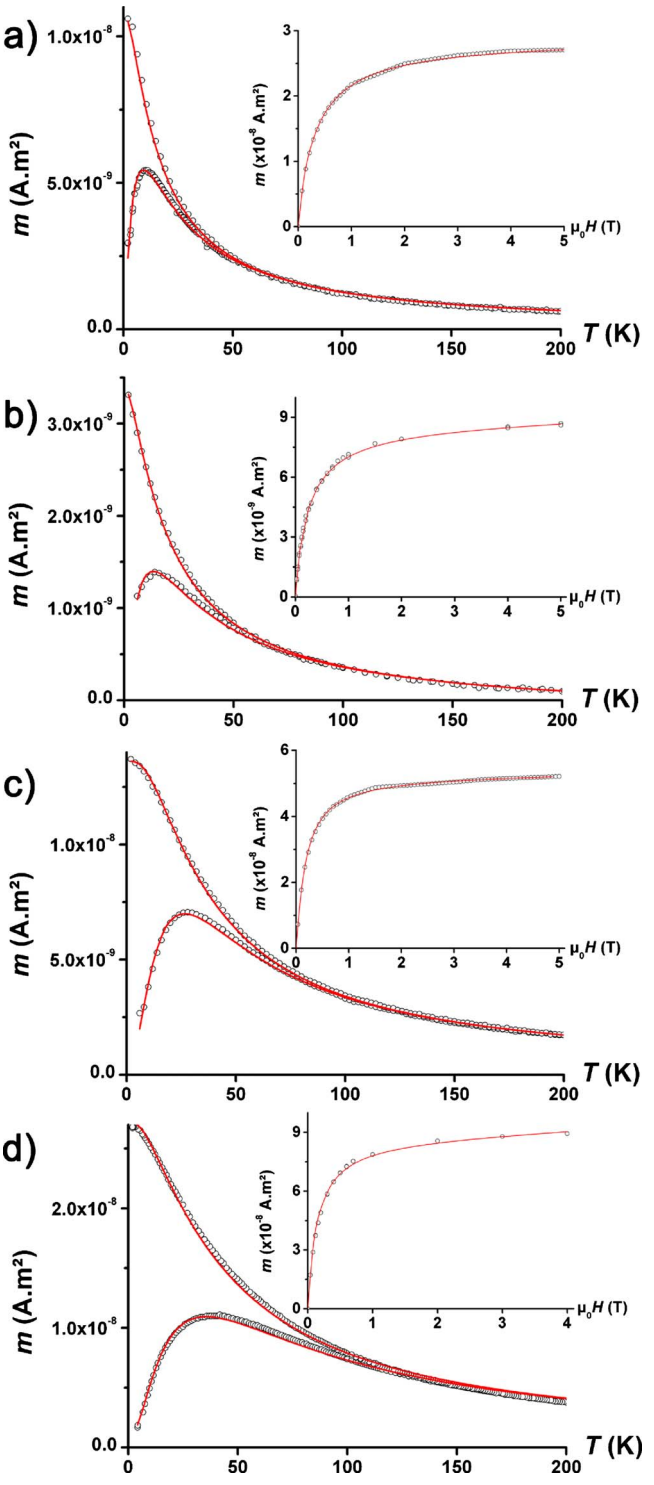

FIG. 4. (Color online) Fig. 2—ZFC/FC curves taken at 5 mT and hysteresis loops at 300 K of the Co clusters embedded in (a) C, (b) Si, (c) Au, and (d) Ag matrices. The solid lines correspond to the adjustments using the triple fit. Variations in signal amplitude are due to variations in sample thicknesses and surface areas.

Note that the mass-selected clusters used for this experiment correspond to a narrow slice cut out of the size distribution as generated in the cluster source. Since this slice

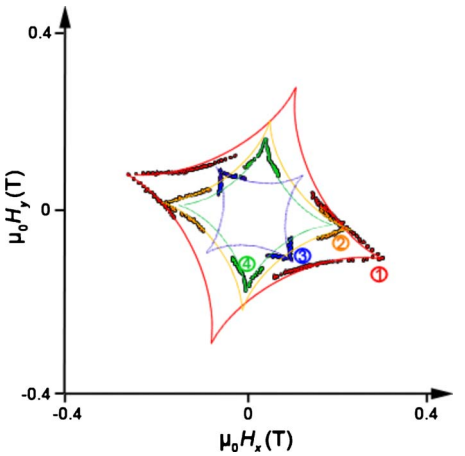

FIG. 5. (Color online) Critical curves of clusters embedded in amorphous carbon matrix at $T=35$ mK. Measurements of clusters in the same μ-SQUID (dots) and fitted astroids (line). The uniaxial anisotropy constants are equal to (1) 194 kJ/m^3; (2) 130 kJ/m^3; (3) 76 kJ/m^3, and (4) 109 kJ/m^3.

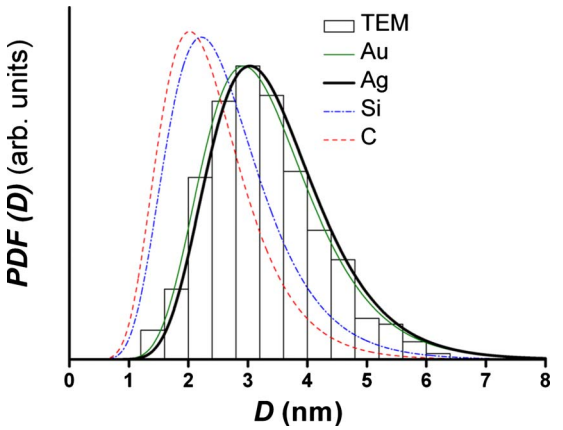

FIG. 6. (Color online) Magnetic diameter PDFs deduced from the fitted ZFC/FC and $m(H)$ curves, for the Au, C, Si, and Ag matrices. The bar plot shows the PDF derived from TEM.

corresponds to a fraction of the large diameter tail of the distribution, an increased mean aspect ratio of around 1.4 has been determined by TEM (Ref. 16) (cf. Fig. 1), as opposed to a mean value of 1.1 for nonsize-selected particles. A possibly increased influence of shape anisotropy with respect to the nonmass-selected distributions is discussed in Sec. IV C.

IV. DISCUSSION

A. Magnetic size distributions

In order to determine the magnetic diameter probability distribution function [PDF(D_{mag})] and the anisotropy constant (K_{eff}) of the Co clusters, we have used the triple fit procedure.[8] In this model, the *entire* ZFC/FC and $m(H)$ curves at 300 K are adjusted simultaneously using a semianalytical model that takes into account the magnetic particles size distribution and the dynamic temperature sweep during the ZFC/FC protocol. The only adjustable parameters are the number of clusters in the sample, those of the magnetic diameter probability distribution function [PDF(D_{mag})] and an effective anisotropy constant (K_{eff}). The corresponding energy barrier of a cluster with a volume V_{mag} is simply written as $E_{ani}=K_{eff}V_{mag}$. The fits to the experimental curves are presented in Fig. 4 whereas Fig. 6 shows the PDFs(D_{mag}) obtained from the adjustments for the four matrices.

(1) Au and Ag matrices: the PDFs(D_{mag}) for Co clusters in Au and Ag matrices are in good agreement with the PDF(D) obtained from electron microscopy as shown in Fig. 6. This result proves that there is no interdiffusion at the Co and Au or Ag interfaces. At the nanometer scale as in the bulk phase Co and Au/Ag are immiscible.[17]

(2) Si matrix: Co clusters in a Si matrix display a PDF(D_{mag}) with a median shifted toward a smaller value as compared to the PDF(D) established by TEM. In the bulk phase, Si and Co are miscible, hinting toward atom exchange at the interface. This interdiffusion can lead to a non magnetic alloy layer and thus a decrease in the magnetic diameter, as previously observed in Nb matrices.[4]

(3) a-C matrix: whereas Co and graphitic carbon are immiscible in the bulk phases, a comparable shift of magnetic median diameter as in the Si matrix is observed. It has to be borne in mind, however, that our samples are not in thermodynamical equilibrium and the formation of a nonmagnetic carbide shell around the cluster cannot be excluded.[18] From the PDF(D_{mag}) and the total number of clusters in the samples, we can directly determine the number of magnetic Co atoms in the sample (1.05×10^{15}) and compare this number to the RBS measurements (2.7×10^{15}). The difference corresponds approximately to 1.5 magnetic dead layers. This result is in good agreement with the difference between the diameter distribution obtained by TEM and the magnetic diameter distribution obtained by the triple fit method and allows us to confirm the existence of a nonmagnetic diffuse interface between Co clusters and the amorphous carbon matrix. The different experimental and adjustment parameters are summarized in Table I.

B. Magnetic anisotropy constants

First of all, it can be seen in Table I that T_{max} does not increase in the same manner K_{eff}. Moreover, the values for Ag and Au matrices show that even a slight variation in the size distribution median can significantly change the ZFC/FC curves and therefore T_{max}. These results underline that using only T_{max} as an indication for the magnetic anisotropy of embedded or deposited nanoparticles is deceptive.[8] In detail, the value T_{max} is defined by the distribution of anisotropy energies of the ensemble of probed particles, which itself depends on the anisotropy constant and the magnetic volume through $E_{ani}=K_{eff}V_{mag}$. The effective anisotropy constant in metallic matrices as derived from the triple fit is larger than that for Si and a-C matrices.

Only minor deviations from spherical shapes have been observed for the nonsize-selected ensembles discussed here (mean aspect ratio of 1.1). Consequently, no shape anisotropy is taken into account in this part of the discussion. Previous investigations have shown that the major contribu-

TABLE I. Maximum of the ZFC susceptibility curves (T_{max}), ratio of remanent to saturation magnetization (m_r/m_s) at 2 K, magnetic anisotropy constant K_{eff}, and magnetic size parameters (median diameter D^m_{mag} and dispersion w) as deduced from triple fit adjustments of SQUID measurements. For comparison, D^m and w as determined from TEM observations are 3.2 ± 0.1 nm and 0.30 ± 0.05, respectively. The last column gives the values of the low-temperature coercivities.

	T_{max} (K)	m_r/m_s at 2 K	K_{eff} (kJ/m^3)	D^m_{mag} (nm)	w	$\mu_0 H_c$ at 2 K (T)
Co:Ag	34	0.42 ± 0.03	174 ± 8	3.3 ± 0.1	0.29 ± 0.02	0.065 ± 0.005
Co:Au	27	0.44 ± 0.03	178 ± 8	3.2 ± 0.1	0.26 ± 0.02	0.07 ± 0.005
Co:Si	14	0.40 ± 0.03	102 ± 5	2.5 ± 0.1	0.34 ± 0.02	0.045 ± 0.005
Co:a-C	10	0.35 ± 0.03	105 ± 5	2.3 ± 0.1	0.33 ± 0.02	0.04 ± 0.005

tion to the cobalt cluster's surface anisotropy comes from additional or incomplete facets of the clusters.[4,5] Therefore, two explanations are possible in order to explain the variation in K_{eff}. On the one hand, atomic intermixing or alloying reduces the crystalline and thus also the magnetic particle diameter. On the other hand, electronic hybridization has been shown to either increase or decrease the magnetic moment and more specifically the orbital moment of interface atoms,[19–22] depending on the detailed chemical and electronic structure at the interface. We will now also consider μ-SQUID measurement on individual mass-selected Co clusters in an a-C matrix.

C. μ-SQUID experiments

According to the Stoner-Wohlfarth model of magnetic anisotropy in two dimensions, the switching field H_{sw} of uniaxial clusters at 0 K along the easy axis directly represents the cluster anisotropy field H_A.[12] This switching field can be measured for different applied magnetic field directions at 35 mK with the μ-SQUID technique. The second-order anisotropy constant term K_u can then be extracted following $\mu_0 H_A = 2K_u/M_s$. Note that at very low temperatures, the switching field does not depend on the nanoparticle size. It can, however, be shown that the anisotropy depends on the detailed crystallinity of the particles and that supplementary facets can induce variations in up to 300 kJ/m^3 (Ref. 4) between clusters with less than 4% difference in the number of atoms. This effect is independent of the demagnetizing shape anisotropy. Consequently, Fig. 5 shows switching field astroids for four individual clusters in the same sample, corresponding to anisotropy values between 76 and 194 kJ/m^3. Note that the use of a μ-SQUID permits a direct verification of the assumption of uniaxial anisotropy and allows the immediate determination of the anisotropy without any assumptions or fit procedures.

This implies that even though interface intermixing can lead to a reduction in the size of the embedded clusters, plus a possible homogenization of particle shapes, considerable variations in K_u remain. Although we must take into account the fact that the increased aspect ratio of the clusters used in this experiment can result in shape anisotropies of the same order of magnitude,[4] we can clearly derive that a magnetically dead layer does not significantly influence the intrinsic dispersion of anisotropies. We attribute this dispersion to additional and/or incomplete facets of the nanoparticles that remain dominant for the magnetic anisotropy despite any matrix effects. We expect electronic effects as well to be most important for the additional facets since their atoms are less coordinated. We cannot, however, at the moment clearly differentiate between the two possible reasons for the reduced magnetic diameter: electronic quenching, atomic interdiffusion, or a combination of the two. To this date no data on the magnetic anisotropy of gas-phase clusters are available, it is thus not possible to differentiate whether the metallic matrices increase the intrinsic anisotropy or whether it is rather the nonmetallic environments that decrease this value. Clearly, theoretical calculations of isolated and embedded magnetic clusters are needed.

Note that the values for K_u as derived from the astroids are in good agreement with the value from the triple fit adjustment, which is a mean over the whole nonsize-selected, more spherical ensemble. This is an indication that shape anisotropy cannot be the dominating contribution to the derived anisotropy of embedded clusters. Preliminary results on size-selected clusters indicate that in fact a certain dispersion of anisotropy constants is needed for a correct reproduction of the magnetization data, a fact that is masked by the still comparably large dispersions of cluster sizes used in the experiments presented here. This observation is in agreement with the observations from micromagnetometry.

V. CONCLUSIONS

We have performed conventional magnetometry experiments on well-defined and interaction-free Co clusters embedded in four different matrices (Ag, Au, Si, and amorphous C) and adjusted the data following our triple fit method. In this way, we extract accurate values for the magnetic size distributions as well as of the magnetic anisotropy constants. These investigations are extended by μ-SQUID experiments on individual size-selected Co clusters in a-C.

We find that the two metallic matrices form neat interfaces with the nanoparticles, the derived diameter distributions are consistent with those determined by electron microscopy. Both Si and a-C matrices reduce considerably the median magnetic diameter of the nanoparticles, either through alloying or electronic quenching. On the other hand,

the two metallic matrices used increase the mean magnetic anisotropy constant by more than 50%.

The micromagnetometry experiments yield large variations in the anisotropy for clusters embedded in a-C. This observation shows that despite all matrix effects, atomic or electronic, the magnetic anisotropy of embedded clusters is still dominated by the detailed shape and crystalline structure of the interface, i.e., additional facets.

ACKNOWLEDGMENTS

This work has been funded through the "Agence National de la Recherche" (ANR DYSC), the "Plateforme Lyonnaise de Recherche sur les Agrégats" (PLYRA), and the "Centre de Magnétométrie de Lyon" (CML). Technical support by C. Albin, C. Clavier, and H. Moutaabid is acknowledged.

*matthias.hillenkamp@lasim.univ-lyon1.fr

[1] *The Physics of Ultrahigh-Density Magnetic Recording*, Springer Series in Surface Sciences, edited by M. Plumer, J. van Ek, and D. Weller (Springer, Berlin, 2001).

[2] V. Skumryev, S. Stoyanov, Y. Zhang, G. Hadjipanayis, D. Givord, and J. Nogués, Nature (London) **423**, 850 (2003).

[3] F. Tournus, A. Tamion, N. Blanc, A. Hannour, L. Bardotti, B. Prével, P. Ohresser, E. Bonet, T. Epicier, and V. Dupuis, Phys. Rev. B **77**, 144411 (2008).

[4] M. Jamet, W. Wernsdorfer, C. Thirion, V. Dupuis, P. Mélinon, A. Pérez, and D. Mailly, Phys. Rev. B **69**, 024401 (2004).

[5] M. Jamet, W. Wernsdorfer, C. Thirion, D. Mailly, V. Dupuis, P. Mélinon, and A. Pérez, Phys. Rev. Lett. **86**, 4676 (2001).

[6] N. Nakajima, T. Koide, T. Shidara, H. Miyauchi, H. Fukutani, A. Fujimori, K. Iio, T. Katayama, M. Nývlt, and Y. Suzuki, Phys. Rev. Lett. **81**, 5229 (1998).

[7] M. Jamet, M. Négrier, V. Dupuis, J. Tuaillon-Combes, P. Mélinon, A. Pérez, W. Wernsdorfer, B. Barbara, and B. Baguenard, J. Magn. Magn. Mater. **237**, 293 (2001).

[8] A. Tamion, M. Hillenkamp, F. Tournus, E. Bonet, and V. Dupuis, Appl. Phys. Lett. **95**, 062503 (2009).

[9] A. Perez, V. Dupuis, J. Tuaillon-Combes, L. Bardotti, B. Prevel, E. Bernstein, P. Mélinon, L. Favre, A. Hannour, and M. Jamet, Adv. Eng. Mater. **7**, 475 (2005).

[10] M. Mayer, "SIMNRA Users Guide," Max-Plank-Institut für Plasmaphysik Technical Report No. IPP 9/113, 1997 (unpublished).

[11] M. Hillenkamp, G. Di Domenicantonio, and C. Félix, Phys. Rev. B **77**, 014422 (2008).

[12] E. Stoner and E. Wohlfarth, Philos. Trans. R. Soc. London, Ser. A **240**, 599 (1948).

[13] R. Alayan, L. Arnaud, A. Bourgey, M. Broyer, E. Cottancin, J. R. Huntzinger, J. Lermé, J. L. Vialle, M. Pellarin, and G. Guiraud, Rev. Sci. Instrum. **75**, 2461 (2004).

[14] C. Raufast, A. Tamion, E. Bernstein, V. Dupuis, T. Tournier, T. Crozes, E. Bonet, and W. Wernsdorfer, IEEE Trans. Magn. **44**, 2812 (2008).

[15] C. Portemont, R. Morel, W. Wernsdorfer, D. Mailly, A. Brenac, and L. Notin, Phys. Rev. B **78**, 144415 (2008).

[16] R. Alayan, L. Arnaud, M. Broyer, E. Cottancin, J. Lermé, J. L. Vialle, and M. Pellarin, Phys. Rev. B **73**, 125444 (2006).

[17] *Binary Alloy Phase Diagramms*, edited by T. Massalski (American Society For Metals, Metals Park, Ohio, 1986).

[18] H. Wang, S. P. Wong, W. Y. Cheung, N. Ke, W. F. Lau, M. F. Chiah, and X. X. Zhang, Mater. Sci. Eng., C **16**, 147 (2001).

[19] P. Gambardella *et al.*, Science **300**, 1130 (2003).

[20] J. Bartolomé *et al.*, Phys. Rev. B **77**, 184420 (2008).

[21] D. Eastham, Y. Qiang, T. Maddock, J. Kraft, J.-P. Schille, G. Thompson, and H. Haberland, J. Phys.: Condens. Matter **9**, L497 (1997).

[22] Xiao Chuanyun, Yang Jinlong, Deng Kaiming, and Wang Kelin, Phys. Rev. B **55**, 3677 (1997).